IEEE Access
Multidisciplinary ⋮ Rapid Review ⋮ Open Access Journal

Received May 26, 2022, accepted June 8, 2022, date of publication June 14, 2022, date of current version June 21, 2022.

Digital Object Identifier 10.1109/ACCESS.2022.3183125

Automatic Obstacle-Crossing Planning for a Transmission Line Inspection Robot Based on Multisensor Fusion

XIANG YUE[1,2], YAN FENG[1], BINZHANG JIANG[1], LIN WANG[3], AND JUNMING HOU[1]

[1]College of Engineering, Shenyang Agricultural University, Shenyang 110866, China
[2]State Key Laboratory of Robotics, Shenyang Institute of Automation, Chinese Academy of Sciences, Shenyang 110016, China
[3]School of Mechanical Engineering, Changshu Institute of Technology, Changshu, Jiangsu 215500, China

Corresponding author: Lin Wang (msewanglin@163.com)

This work was supported in part by the National Natural Science Foundation of China under Grant 51605311, and in part by the Youth Program of Liaoning Education Department under Grant LSNQN202025.

ABSTRACT Accurate obstacle detection and proper behavior planning are key factors in the success of transmission line inspection robots. To achieve the autonomous location and identification of line obstacles in the operation of transmission line inspection robots, we propose a method in which information from various sensors is used to control a robot such that it can reliably and stably approach, locate, and identify obstacles. The accuracy and real-time requirements of obstacle information in the autonomous operation of the inspection robot are analyzed, a multi-sensor integrated structure for line obstacle location and identification is proposed, and an obstacle location and identification algorithm is designed for each stage. The principle of monocular vision ranging is used to control the robot such that it approaches obstacles and enters the short-range location stage, where the reliable location of obstacles is achieved via collision-encoder-current sensor data fusion. Obstacles are identified and the identification results are combined with those of the approaching rolling phase. The robot state vector is constructed according to the obstacle detection information and information measured by the robot sensors. Based on the current state vector, combined with the robot obstacle surmounting process, an obstacle surmounting behavior planning method based on multi-sensor fusion is implemented. Experiments were conducted using laboratory-simulated lines to verify the effectiveness of the proposed method for obstacle detection and behavior planning during transmission line inspection.

INDEX TERMS Inspection robot, identification, location, multi-sensor fusion, planning.

I. INTRODUCTION

Power transmission lines must be scrutinized because the failure of these systems leads to serious consequences. The means of inspection and maintenance must evolve to address grid operator challenges such as aging assets, stricter regulations, and high reliability standards. Power line robots are promising for the advancement of maintenance practices [1]–[4]. Generally, a power transmission line environment can be described as a semi-structured environment in which the autonomous motion control of inspection robots is difficult to achieve [5].

During the inspection of power transmission lines, electric power fittings such as vibration dampers, suspension clamps, and tension clamps increase the difficulty for navigating on the line efficiently and stably. Obstacle recognition and localization become important development directions for power transmission line inspection robots. Obstacle identification and localization methods based on a global positioning system and prior line knowledge can provide global information regarding the line environment [6]. Rui *et al.* proposed a novel mobile robot prototype for the inspection of overhead transmission lines [7]. It can roll over certain obstacles (compression splices, vibration dampers, etc.). The robot can clear other types of obstacles (spacers, suspension clamps, etc.). Zhu *et al.* proposed a gibbon-like crawling inspection robot using the bionic design method and analyzed the climbing behavior of gibbons [8]. This robot can swing a cantilever on a high-voltage transmission line to realize crossing of the drain line. A one-wheel-drive low-cost power line inspection

The associate editor coordinating the review of this manuscript and approving it for publication was Okyay Kaynak.

robot called ''ROSETLineBot'' was developed in 2019 [9]. It is crucial to detect and diagnose possible problems on lines before they develop?. Zhu *et al.* designed an inspection and foreign body removal robot walking on twin bundle conductors that can move over spacers and counterweights directly and quickly [10]. A novel crawler-type robot was presented in Ref. [11]. This robot is composed of three arms and a balance mechanism, which are all joined together through a base. The crawler-type inspection robot is an attempt to develop a novel robot structure for high-voltage power transmission line inspection.

Reference [6] presented the characterization of a laser range finder applied to obstacle detection in power line conductors. Methods based on ranging sensors can recognize obstacles and their initial positions in a local environment. However, they cannot realize the location and recognition of obstacles in a global environment. Le *et al.* proposed a novel method based on binocular vision to extract the feature points of images and reconstruct three-dimensional scenes [12], [13]. Li Zhenhui *et al.* developed a structure-constrained obstacle recognition algorithm using machine vision sensors [14]. Vision sensors provide a large amount of environmental information, but their algorithms generally have a large amount of data and complex operations, and it is challenging to ensure real-time performance. Heng *et al.* proposed a method for obstacle detection and location based on multisource information and behavior [15].

The reliable location and identification of line obstacles is key to ensuring the safe operation of inspection robots and realizing autonomous obstacle crossing. Obtaining comprehensive and accurate environmental information using a single sensor is difficult. Therefore, multi-sensor fusion technology plays an important role in improving the ability of inspection robots to locate and identify obstacles.

The Canadian Hydro-Quebec Research Institute [16], [17] designed the LineScout robot, which utilizes a mode-operation strategy and joint sensor information. Based on the restriction that the configurations at the beginning and end of movement should correspond exactly, control difficulty lies not only in moving the arm frame to an appropriate thread-catching position, but also in making the two arms simultaneously and reliably grasp a thread. To avoid complex kinematic equations, Hibot Corporation [18] designed an Expliner robot to read information from each joint sensor. The difficulty of control lies in reliably lifting the walking wheel for obstacle avoidance and the requirement for a single walking wheel must be satisfied. The entire robot must be balanced when the wheel is on a power line. Wuhan University [19] established a robot collision avoidance model based on known obstacle information in which obstacles were identified and local attitude adjustments were planned through electromagnetic sensor groups. The Shenyang Institute of Automation of the Chinese Academy of Sciences [20], [21] studied motion-planning methods for a distributed expert system and a generative system for two types of inspection robots. Additionally, the Federal University of Uberlandia and the Institute of Automation of the Chinese Academy of Sciences [16], [17] designed corresponding force-planning methods for the robots they developed. In general, current motion-planning methods for inspection robots are aimed at different types of mechanisms and combined with kinematic models or joint sensor information to solve the obstacle-crossing problem. There is no universal and unified force-planning method.

The supervisory control theory of discrete-event dynamic systems (DEDS), which was first introduced by Ramadge and Wonham, is based on the automata concept. Given a process, the objective of this theory is to design a supervisor such that the process coupled with the supervisor behaves according to various constraints [22]. In Refs. [23], [24], a DEDS monitoring theory based on automata was proposed and the interaction and evolutionary relationships between events and states were studied. Yifeng *et al.* studied the behavior planning of a repair robot based on vision [25]. Huang Le *et al.* proposed a finite-state machine (FSM) model for a robot autonomous behavior control method [13]. This FSM easily links a planning method based on sensors and expert system to realize automatic control.

The goal of obstacle-crossing planning for inspection robots is to describe complex obstacle-crossing motions uniformly and obtain a formal expression to realize the automatic reasoning and automatic obstacle crossing of robots. An appropriate movement mode is selected according to the environmental conditions and obstacle type, and obstacle crossing is completed. Robots must automatically adapt to changes in environmental factors using sensory information and evaluate their security status. According to the robot's external sensors, including vision and pose sensors, the advantages and disadvantages of obstacle categories and environmental conditions in the environment are determined and a motion mode is selected.

This study focused on obstacle-crossing planning for inspection robots based on multi-sensor fusion. Section II reviews the operational context inherent to power utilities, mechanical structure of the target robot, and multi-sensor system. Section III presents the algorithm used to locate and distinguish obstacles. Section IV presents different aspects of obstacle-crossing planning based on a Finite State Machine (FSM). The behaviors of the robot are analyzed and modeled using FSM. The details are given and the simulation is conducted. Section V presents an experimental test, which verifies the correctness of the proposed recognition algorithm and feasibility of obstacle-crossing planning. Section VI concludes this paper and discusses future research work

II. TECHNOLOGY DESIGN

A. TYPES AND SEQUENCES OF OBSTACLES

A general schematic of an overhead transmission line is presented in Figure 1. According to the inspection task requirements for power transmission lines, the robot must roll on the overhead ground wire (OGW), navigate obstacles, and carry

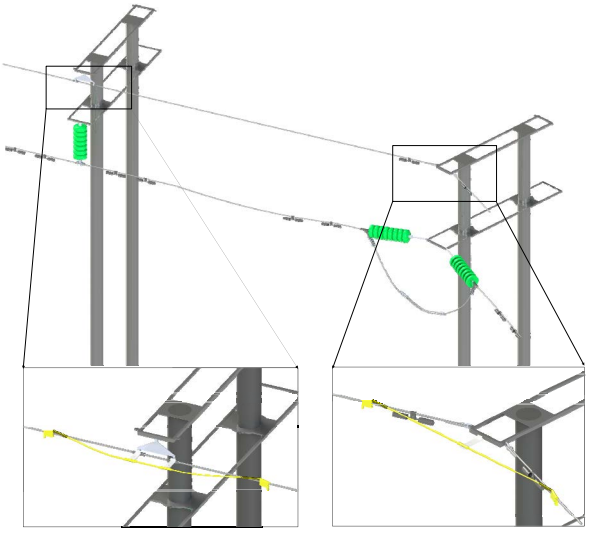

FIGURE 1. Environment of a 110 kV transmission line.

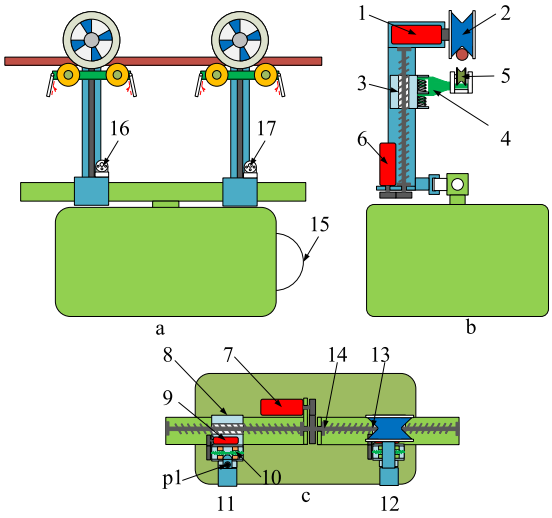

FIGURE 2. Structure of the robot.

a visible-light camera and an infrared camera to accomplish inspection tasks. The OGW is suspended from a suspension tower using a suspension clamp that is connected to a strain tower by a stain clamp. Vibration dampers installed near towers have various shapes and sizes. Numerous other types of obstacles may also be present in a given network. Obstacles are mounted on the OGW in sequences at certain distances that separate one obstacle from the next.

To accomplish inspection tasks, the robot must be able to navigate around obstacles near the suspension towers and strain towers. Current robots navigate obstacles by imitating the cantilevered climbing maneuvers of apes. The efficiency of this obstacle-crossing method is generally low. In this study, a bridge track was added to the two ends of the tension tower and linear tower, connecting the ground wires at both ends. The rolling wheel was designed to be sufficiently large to roll directly over the damper during the design process. Therefore, the robot has an unobstructed ground wire road structure and the efficient and safe inspection of the entire line can be realized.

B. MECHANICAL DESIGN

Figure 2 presents a structural schematic of the robot. An aerial earth wire? is used as a support. The wheels of the robot allow it to move quickly and efficiently along a power line and roll over obstacles (compression splices and vibration dampers). The robot consists of three independent assembly units (Figure. 2(a)), i.e. two locomotion mechanism units including one motorized rubber wheel called the ''rolling mechanism'' and two passive nylon pulleys called the ''clamping mechanism''; a center unit, which connect the first two units and allow them to slide and pivot; and box units.

As shown in Figure 2(b), a brushless DC motor (1) coupled to a planetary flanged-output gearbox directly supports the traction wheel (2). The gripper plate (4) is connected to a nut (3) on the trapezoidal screw and it is possible to move the grippers (5) vertically by rotating the trapezoidal screw using the motor (6). When an obstacle is reached, the grippers are moved to the bottom such that the traction wheel can roll over the obstacle.

The center unit supports 50% of the total weight while providing both translational and rotational degrees of freedom. As shown in Fig. 2(c), two locomotion mechanism units are mounted on two machined plates (10 and 11) and can be locked using a sector of the two-way trapezoidal screw (11) actuated by a DC motor (9). The robot can roll on a curve after the locomotion mechanism units are unlocked. The screw nuts (8 and 13) are mounted on a two-way trapezoidal screw (14) and moved by a DC motor (7). Because the left and right sides of the two-way trapezoidal screw have different rotation directions, the screw nut meshes on different sides of the two-way trapezoidal screw. Therefore, translations occur in opposite directions.

C. MULTI-SENSOR SYSTEM

The inspection robot's multi-sensor system consists of internal sensors (encoders, current sensors, temperature sensors, limit sensors, inclination sensors, battery-power sensors, etc.) that indicate the state of the robot and external sensors (vision and contact sensors) that sense the environment. An encoder, a current sensor, a temperature sensor, and a limit sensor are installed at each joint motor to determine the state of each joint of the robot. The inclination sensor feeds back the overall inclination angle of the robot. A battery power sensor is used to detect and estimate the remaining battery power of the robot. Contact sensors are installed at the front and rear ends of the gripper. The vision sensor includes a pan-tilt-zoom (PTZ) camera (15) installed at the front of the robot and a pinhole camera (16, 17) under the two locomotion mechanisms. The PTZ, pinhole, and contact sensors are used for the location and recognition of the environment in front of the robot.

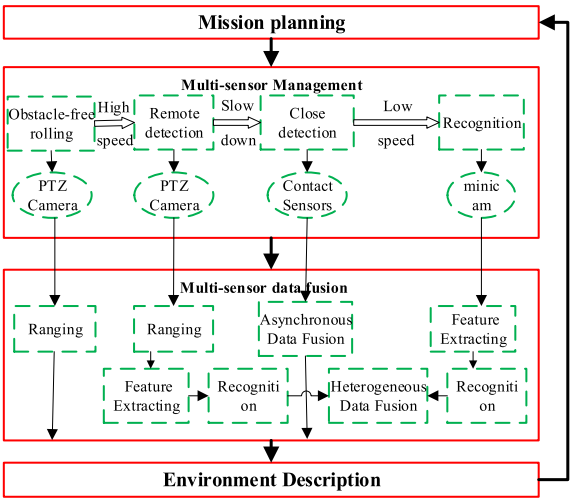

FIGURE 3. Robot multi-sensor system.

In this study, a multi-sensor system structure presented in Figure 3. was designed to satisfy the requirements of sensor perception range, accuracy, and real-time performance for the location and identification of obstacles by the inspection robot. The target task planning layer plans the current target task of the robot according to its environment and state. The target tasks mainly include rolling without obstacles, approaching rolling with obstacles, locating obstacles at a close range, and identifying obstacles. The sensor coordination manager coordinates sensors according to the target task. The sensor data processing and fusion layers are responsible for sensor information collection, preprocessing, and the fusion and transmission of asynchronous information between subsystems. The environment description layer is responsible for converting the sensor fusion results into environmental parameters and passing them to the robot target planning layer.

When the robot is running at a high speed, grayscale segmentation is applied to the front-end camera images to extract areas where there may be obstacles. If there are no suspicious obstacles in the current field of view, the robot performs the task of rolling without obstacles. Otherwise, the robot performs a rolling task with obstacles. The approaching rolling task is performed when the robot approaches an obstacle and it uses the pan-tilt camera monocular vision ranging method to determine the distance to the obstacle area. Its movement speed is controlled according to the distance such that it approaches the obstacle area stably. When the distance reaches a specific value, the robot triggers a low-speed and short-distance obstacle location task and performs feature extraction on the current obstacle area. In the low-speed and short-distance obstacle location task, the robot uses the encoder, current sensor, and contact sensor fusion information to locate obstacles accurately. After the touch sensor is triggered, the obstacle is in the field of view of the pinhole camera under the forearm. The current obstacle is recognized based on the wavelet-invariant moment features of the pinhole camera images. The results are fused with the decision to identify the current obstacle to determine the next obstacle-surmounting strategy.

III. OBSTACLE LOCATION AND RECOGNITION

A. OBSTACLE LOCATION ALGORITHM

In robot inspection, it is necessary to extract features and measure distances for areas that may contain obstacles. In the task of rolling without obstacles, the environmental information required for the robot's decision making is simply whether there are obstacles in front of the robot, necessitating real-time performance with low precision. In the task of approaching rolling with obstacles, the environmental information required for robot decision making is the distance between the robot and obstacle, which requires real-time performance and high accuracy.

Monocular vision geometric optics ranging is used to measure the distance to the target in an image according to the perspective principle and focal length of the image acquisition equipment. Monocular ranging uses the feature that the camera and measured point are in the same plane. The camera parameters and set transformation are defined in this plane and the transformation relationship between the image pixel coordinates and actual coordinates is calculated. The horizontal distance from the suspicious area of the obstacle to the robot end with the PTZ camera is defined as the obstacle location distance. As shown in Fig. 4, the optical axis of the camera passing through lens O intersects with the power line. The horizontal and vertical distances between the anti-vibration hammer and the camera are denoted as D and H, respectively. According to the principle of pinhole imaging, we obtain

$$\begin{cases} \tan\alpha = x/f \\ \tan(\alpha+\beta) = H/D \end{cases}. \tag{1}$$

When the robot rolls forward by ΔD, (1) is transformed into

$$\begin{cases} \tan\alpha' = x'/f \\ \tan(\alpha'+\beta) = H/(D-\Delta D) \end{cases}, \tag{2}$$

where x and x' represent the pixel offsets and β represents the horizontal angle of the camera. From (1) and (2), the horizontal and vertical distances from the current obstacle area are $D-\Delta D$ and H, respectively. The rolling speed of the robot can be controlled by $D-\Delta D$ to approach the obstacle smoothly. The feature values (area, aspect ratio, etc.) of the obstacle are calculated as the robot approaches the obstacle and are used for the fusion of decisions.

When a robot performs the task of short-range obstacle location, the obstacle location algorithm requires high precision and good real-time performance. In this task, detection results are obtained through the fusion of different types of sensor information to locate obstacles. For the proximity location of obstacles, the fusion of data from contact sensors, encoders, and current sensors is adopted. The data collection

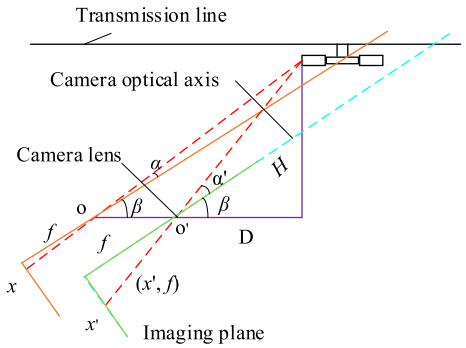

FIGURE 4. Camera imaging diagram.

and processing speeds of these three sensors are high, which ensures the real-time performance of the algorithm, and the fusion of data from multiple sensors increases location accuracy. Contact sensors are installed at both ends of the walking wheel and can identify collisions between the robot and line obstacles. An encoder is installed on the rolling motor shaft of the walking wheel to detect the speed of the motor in real time. The motor current sensor detects the rolling current of the walking wheel. When the walking wheel in front of the robot touches an obstacle, the outer contact sensor of the front wheel is triggered first. Then, based on the resistance of the traveling wheel, the motor torque of the traveling wheel increases and the motor speed decreases.

When the robot encounters an obstacle, the contact sensor is triggered in real time. However, in a field environment, the contact sensor may be falsely triggered by jitter, deformation points, and line protrusions. Therefore, a method of continuous detection is adopted to prevent false detections. The average output value for i consecutive detections after the touch sensor is triggered for the first time is defined as follows:

$$A_i = A\,(1) \cdot A\,(2) \cdot \ldots \cdot A\,(i)\,, \tag{3}$$

where $A\,(i) = \begin{cases} true & \text{The i}^{\text{th}}\text{detection sensor is triggered} \\ false & \text{The i}^{\text{th}}\text{detection sensor is not triggered} \end{cases}$

This method overcomes the false detections caused by shaking of the robot. Considering the changing laws of the current and rotational speed of the rolling motor of the walking wheel when the robot encounters an obstacle, three different types of sensor data can be fused to locate the obstacle accurately.

The comprehensive value of the encoder sensor for i consecutive detections after B_i triggering is given by

$$B_i = B\,(1) \cdot B\,(2) \cdot \ldots \cdot B\,(i) \tag{4}$$

where $B\,(i) = \begin{cases} true & v\,(i) - v\,(i-1) < -v_{ref} \\ false & else \end{cases}$, with $v(i)$ representing the motor speed at the i^{th} detection.

The average value of the current sensor for i consecutive detections after A_i triggering is given as

$$C\,(i) = [C_i\,(1) + C_i\,(2) + \ldots + C_i\,(n)]\,/n \tag{5}$$

where $C_i\,(n)$ represents the n^{th} detection value of the sensor. The comprehensive output state value of the current sensor is expressed as

$$C_i = \begin{cases} true & C\,(i) - C\,(i-1) > C_{ref} \\ false & else \end{cases} \tag{6}$$

where X_i represents the detection status. The fusion result is

$$X_i = A_i \cdot B_i \cdot C_i.$$

When $X_i = true$, it can be judged that the obstacle is in contact with the walking wheel of the robot.

B. OBSTACLE RECOGNITION

When the robot performs obstacle recognition, obstacle classification can be conducted using the image features of the pinhole camera under the arm. The most common obstacles in line environments are clamps and vibration dampers. The wavelet moment features of image edges were used in this study to classify obstacles. The wavelet moment invariant of image edges has the characteristics of translation, rotation, and scale factor invariance, and can be used to obtain the global and local features of an image simultaneously. Therefore, it has a high recognition rate for similar objects. The primary identification methods are defined as follows.

1) Preprocess the images collected by the pinhole camera.
2) Extract edges from the image using the Canny operator.
3) The optimal wavelet moment features of the edge images are extracted and a classifier is designed for classification and recognition.

We introduce a set of wavelet moment invariants for classifying objects, which are defined as follows:

$$\left\|F_{m,n,q}\right\| = \left\| \int \int f\,(r,\theta)\,\varphi_{m,n}\,(r)\,e^{jq\theta} r dr d\theta \right\| \tag{7}$$

where $q = 0, 1, 2\ldots$, $m = 0, 1, 2\ldots$, and $n = 0, 1, \ldots, 2^{m+1}$. Different m, n, and q values can be selected to obtain image features at different scales. The polar coordinates of the image function $f\,(x, y)$ are expressed as $f\,(r, \theta)$.

To obtain rotation-invariant moments, the following generalized expression is typically used:

$$\varphi_{a,b}\,(r) = \frac{1}{\sqrt{a}}\varphi\left(\frac{r-b}{a}\right) \tag{8}$$

where a is a dilation parameter and b is a shifting parameter. The mother wavelet $\varphi(r)$ of the cubic B-spline in the Gaussian approximation form is

$$\varphi\,(r) = \frac{4a^{n+1}}{\sqrt{2\pi\,(n+1)}}\sigma_w \cos\left(2\pi f_0\,(2r-1)\right) \exp\left(-\frac{(2r-1)^2}{2\sigma^2\,(n+1)}\right) \tag{9}$$

Because the image size is always restricted to a domain $\{r < 1)$, both a and b are set to 0.5 and the domains for m and

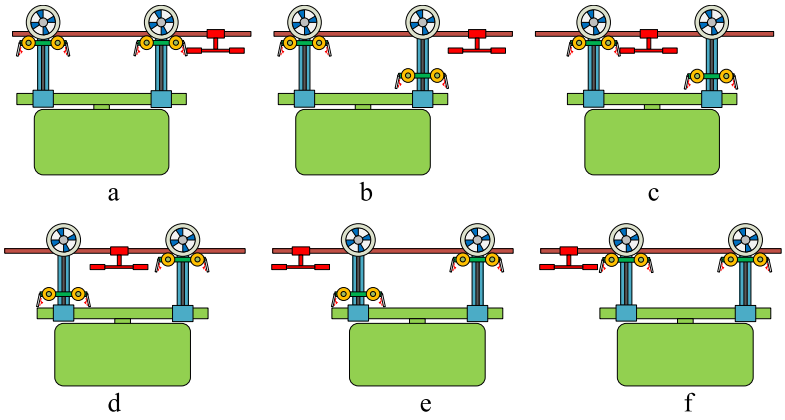

FIGURE 5. Damper navigation sequence.

n are restricted as follows:

$$\begin{cases} a = 0.5^m, \\ b = 0.5 \cdot n \cdot 0.5^m, \\ m = 0, 1, 2, 3 \\ n = 0, 1, \ldots, 2^{m+1}. \end{cases} \tag{10}$$

Then, the wavelet defined along a radial axis in any orientation is denoted as

$$\varphi_{m,n}(r) = 2^{\frac{m}{2}} \varphi\left(2^m r - 0.5n\right) \tag{11}$$

The extracted wavelet moment features at different scales are selected using the l-r method in the suboptimal search algorithm and the n best wavelet moment eigenvalues are selected and normalized as the classifier input.

Obstacle classification and recognition fuse classification results based on the area and aspect ratio features of the PTZ camera and classification results of the wavelet-invariant moment features of the obstacle edges from the pinhole camera under the arm in the trigger stage of the contact sensor to increase obstacle recognition accuracy. The similarity measure between sample x and C_i is expressed as follows:

$$\sigma_i = \frac{1}{\|x - C_i\|} = \frac{1}{\sqrt{\sum \left(x_j - c_j\right)^2}} \tag{12}$$

where x_i and c_i represent the j^{th} eigenvalues of samples x and c, respectively.

The probability that sample x belongs to class C_i is

$$p(x/C_i) = \frac{\sigma_i}{\sigma_1 + \sigma_2 + \sigma_3} \tag{13}$$

Considering the obstacle area and its aspect ratio as the feature values of the PTZ camera, the probability that sample x belongs to class C_i is $p_s(x/C_i)$. Considering the wavelet-invariant moments of the obstacle edges from the pinhole camera under the arm as feature values, the probability that sample x belongs to class C_i is $p_f(x/C_i)$. Then, the probability that sample x belongs to class C_i is defined as

$$p_e(x/C_i) = \sqrt{p_s(x/C_i) * p_f(x/C_i)} \tag{14}$$

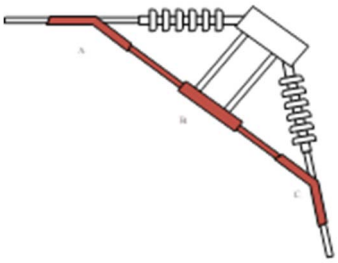

FIGURE 6. Auxiliary rail mounted on the tension tower.

If $p_e(x/C_i) > \sum_{j \neq i} p_e(x/C_j)$, then sample x belongs to class C_i.

IV. BEHAVIOR PLANNING

A. STRATEGY FOR NAVIGATING OBSTACLES

1) NAVIGATING A DAMPER

The robot decelerates when the counterweight on a damper is detected by the vision system of the robot control system and stops when the approximate switch mounted on the front locomotion mechanism is triggered, as shown in Figure 5(a). The clamping mechanism is then driven to the home position, as shown in Figure 5(b). Additionally, the rolling mechanism of the locomotion mechanism drives the robot forward and the robot navigates the damper directly. The robot continues rolling until the approximate switch mounted on the rear locomotion mechanism is triggered, as shown in Figure 5(c). Subsequently, the front clamping mechanism clamps the ground line. Thereafter, the rear clamping mechanism moves to its home position, as shown in Figure 5(d). The robot starts to move forward, which enables the rear locomotion mechanism of the robot to navigate the damper directly, as shown in Figure 5(e). The rear clamping mechanism then clamps the ground line and the robot finishes navigating the damper, as shown in Figure 5(f).

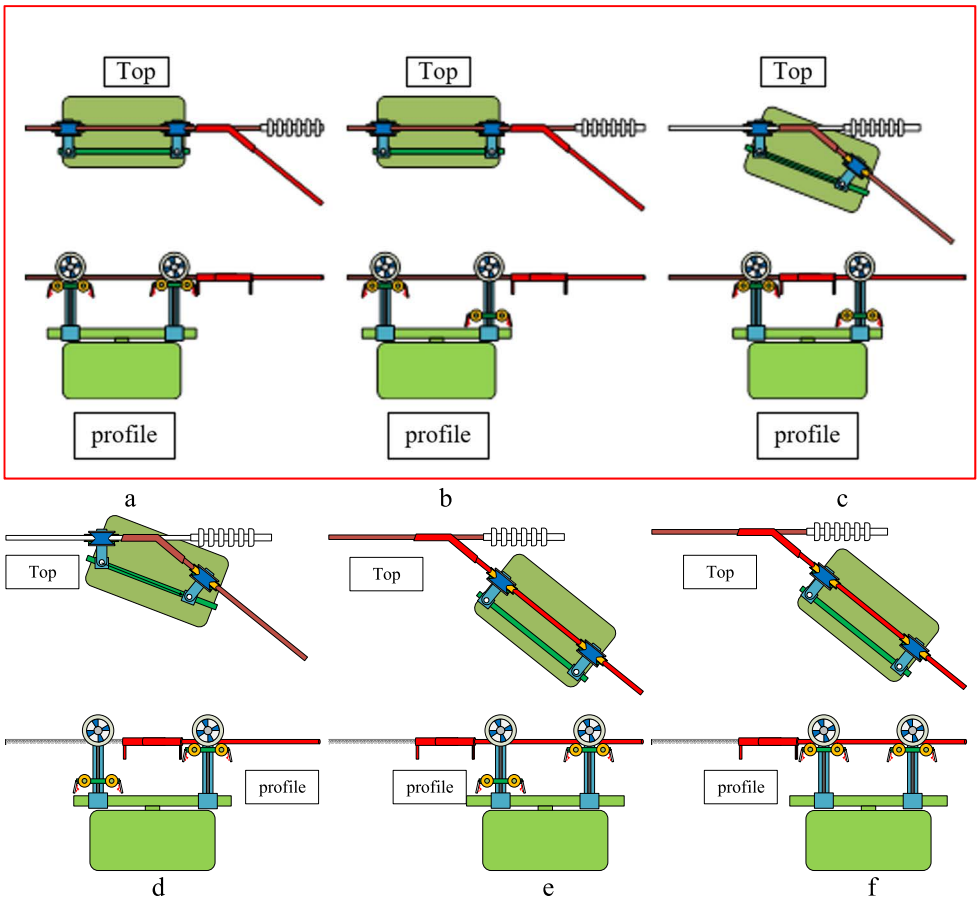

FIGURE 7. Procedure for navigating segment A of the rail.

2) NAVIGATING A TENSION TOWER

The inspection robot can navigate a tension tower with the aid of an auxiliary rail, which is manually mounted on the ground line. The rail is composed of several segments connected by joints. Both ends of the rail are fixed to the ground line and the joints are fixed to the tension tower using brackets, as shown in Fig. 6. Each segment is equipped with two barriers to trigger the sensor.

The auxiliary rail consists of three segments and the actions taken to navigate segment B are similar to those taken to navigate a damper. Clearly, the sequence for navigating segment A is similar to that for navigating segment C. Therefore, the sequence for navigating segment A is considered as an example, as shown in Figure 6.

The robot travels along the ground line and stops when the approximate switch mounted on the front locomotion mechanism is triggered by the flipper located on segment A of the rail, as shown in Figure 7(a). Subsequently, the front locomotion mechanism is released by rolling the locking mechanism and the front clamping mechanism returns to its home position, as shown in Figure 7(b). The robot resumes rolling and navigates the junction of the auxiliary rail and ground line, and it stops when the barrier is detected by the approximate switch mounted on the rear locomotion mechanism, as shown in Figure 7(c). Subsequently, the front clamping mechanism clamps the ground line and the rear clamping mechanism returns to its home position. The rear locking mechanism is then released and the front locking mechanism locks the front locomotion mechanism. Figure 7(d) presents the state of the robot at this point. The robot moves forward until the approximate switch on the front locomotion mechanism is triggered by the barrier mounted on segment B of the rail, as shown in Figure 7(e). Finally, the rear clamping mechanism clamps the ground line and the robot finishes navigating segment A, and is ready to navigate segment B of the auxiliary rail, as shown in Figure 7(f).

B. BEHAVIOR PLANNING FOR THE ROBOT

1) BEHAVIOR OF THE ROBOT

The actions taken by the robot depend on the outputs of the sensors, meaning there is tight coupling between sensing and acting. Behavior-based robotics are useful for ensuring robustness under uncertain circumstances. During its operation, the inspection robot constantly executes behaviors such as ''drive the front clamping mechanism to its home position'' or ''release the front locomotion mechanism.'' In this study, an FSM was used to sequence these behaviors.

TABLE 1. Basic behaviors.

Name	Meaning
BB_FC_ReturnHome	Front clamping mechanism returns to its home position
BB_FC_Clamping	Front clamping mechanism clamps the ground line
BB_FL_Release	Front locking mechanism releases the front locomotion mechanism
BB_FL_Lock	Front locking mechanism locks the front locomotion mechanism
BB_BC_ReturnHome	Rear clamping mechanism returns to its home position
BB_BC_Clamping	Rear clamping mechanism clamps the ground line
BB_BL_Release	Rear locking mechanism releases the rear locomotion mechanism
BB_BL_Lock	Rear locking mechanism locks the rear locomotion mechanism
BB_F_Rolling	Rolling mechanism drives the robot forward

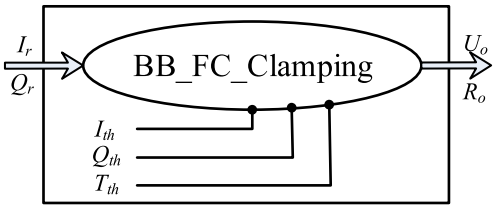

FIGURE 8. Sketch diagram of BB_FC_Clamping.

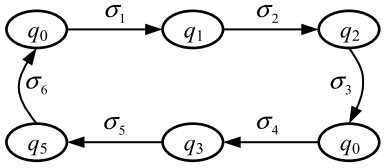

FIGURE 9. FSM for the behavior of navigating a damper.

The behaviors of the inspection robot can be divided into simple and complex states, and they can be modeled as basic and combinational behaviors. Basic behaviors are related to execution mechanisms and can be considered as actions. Table 1 lists the basic behaviors of the inspection robot.

The basic behavior can be expressed using port automata [26] as follows:

Basic Behavior := [behavior name:<name>,
input port list:(<iplist>),
ouput port list:(<oplist>),
parameter list:(<paralist>),
behavior body(<body>)]

where behavior name is necessary and other parameters in the parentheses are optional.

Some basic behaviors are related to specific parameters while others are not. For example, BB_FC_Clamping, which is used to clamping the ground line for the front clamping mechanism, has three parameters, two input ports and two output ports. I_{th} is the threshold current for the front clamping mechanism to clamp the ground line, Q_{th} is the threshold incremental value of the encoder mounted on the motor and T_{th} is the time when a timeout event occurs. I_r is the actual current obtained by the driver of the motor and Q_r is the incremental value of the encoder when the front clamping mechanism is clamping the ground line. U_o is the voltage of the motor and R_o is result of the behavior.

When the front clamping mechanism starts to act, the current of the driver of the motor is obtained every 10ms. The behavior is successful if I_r is larger than I_{th} for a given time and if Q_r is larger than Q_{th}. The behavior is unsuccessful if the execution time is larger than T_{th}, which means some exceptions happen and human interference is needed. The exceptions may due to mechanical error or sensor error and R_o can be used to diagnose the exceptions of the behavior. I_{th}, Q_{th} and T_{th} are determined by conducting experiments.

Combinational behavior is composed of several basic behaviors and inferences. An inference refers to a decision based on sensor information and the current state of the robot. The combinational behaviors of the robot include navigating the damper and tension tower through an auxiliary rail and can be modeled using an FSM, which can be expressed as follows:

$$M = \{Q, \Sigma, \delta, q_0, F\} \tag{15}$$

Here, Q is a non-empty set of states, $q_i \in Q$ is a state, $q_0 \in Q$ is the default state, Σ is a finite set of input events, $\sigma_i \in \Sigma$ is an input event of M, δ is a transition function, and F is a set of final states of M ($F \subseteq Q$).

The combination behavior is also related to some parameters as exceptions may happen in the field, and the parameter is helpful for the operator to diagnose the error if an exception occurs.

2) BEHAVIOR PLANNING FOR NAVIGATING A DAMPER

When the approximate switch mounted on the front clamping mechanism encounters a damper, the vision system takes photographs using a camera and then begins to recognize the obstacle. After the damper is recognized, the robot takes several steps to navigate it, as shown in Figure 8. For safety purposes, at least one clamping mechanism should clamp the ground line at all times. The basic states are listed in Table 2.

The behavior for navigating a damper can be modeled using an FSM, as shown in Figure 9. The events generated by the sensor inputs and control system are listed in Table 3.

TABLE 2. Basic states related to navigating a damper.

Name	Meaning	Figure	State
R_Navigating	The clamping mechanism clamps the ground line and the locking mechanism locks the joints. The robot is not rolling.	Fig. 6(a)	q_0
R_Navi_S1	The front clamping mechanism returns home while the rear clamping mechanism clamps the ground line. The locking mechanism locks the joints. The robot is not rolling.	Fig. 6(b)	q_1
R_Navi_S2	The front clamping mechanism returns home while the rear clamping mechanism clamps the ground line. The locking mechanism locks the joints. The robot is rolling.	Fig. 6(c)	q_2
R_Navi_S3	The rear clamping mechanism returns home while the front clamping mechanism clamps the ground line. The locking mechanism locks the joints. The robot is not rolling.	Fig. 6(d)	q_3
R_Navi_S4	The rear clamping mechanism returns home while the front clamping mechanism clamps the ground line. The locking mechanism locks the joints. The robot is rolling.	Fig. 6(e)	q_4
R_Traveling	The clamping mechanism clamps the ground line and the locking mechanism locks the joint. The robot is rolling.	Fig. 6(f)	q_5

TABLE 3. Events of the behavior for navigating a damper.

Event name	Meaning
σ_1	The approximate switch at the home position of the front clamping mechanism is triggered.
σ_2	Robot command: start the robot.
σ_3	The forward approximate switch of the rear clamping mechanism is triggered.
σ_4	The approximate switch at the home position of the rear clamping mechanism is triggered.
σ_5	Robot command: start the robot.
σ_6	A given time elapses.

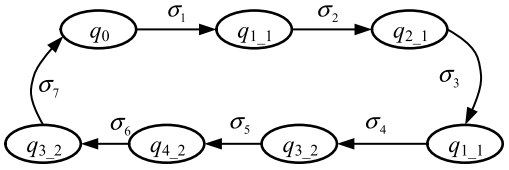

FIGURE 10. FSM of the behavior for navigating the first segment of a rail.

3) BEHAVIOR PLANNING FOR NAVIGATING A TENSION TOWER

The behavior of the robot for navigating a tension tower is far more complex than that for navigating a damper. However, the process of navigating a tension tower is similar to that of navigating a damper. There are two main differences. The robot navigates a tension tower by repeating the process for navigating a damper three times. The locking mechanism should act as an auxiliary rail, which is not straight. The first segment is considered as an example. Table 4 lists the basic behaviors related to the navigation of a tension tower.

The behavior for navigating the first segment of a rail was modeled using an FSM, as shown in Figure 10. The events generated by the sensor inputs and control system are listed in Table 5.

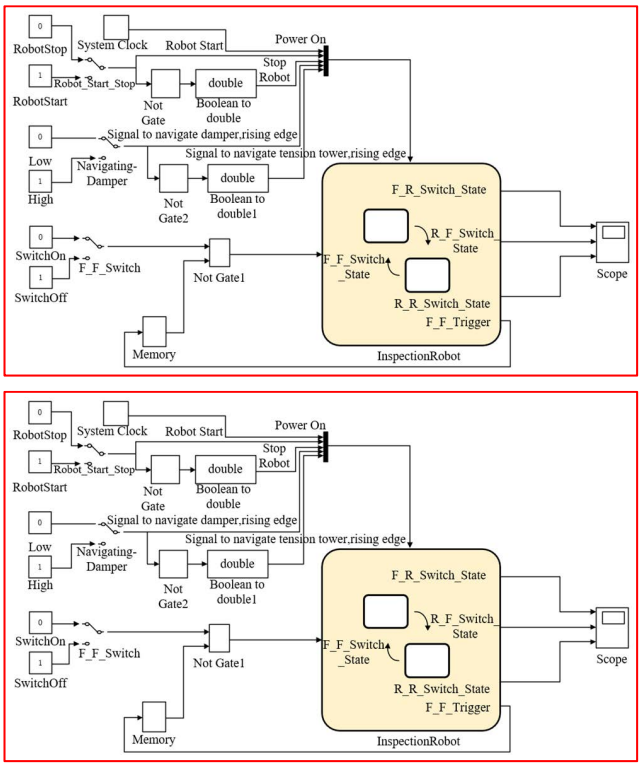

FIGURE 11. Behavior planning model for the inspection robot.

4) EXCEPTION HANDLING MECHANISM

The ground line on which the robot travels is very complicated in the field and some unexpected exceptions may happen. Thus, the supervision of an operator is necessary to ensure the safety of the robot. For example, when the basic behavior is running, mechanical error or sensor error may happen, which results to a failure of the basic behavior. Thus the robot is not able to navigate the obstacle automatically. The exception handling mechanism is designed to deal with

TABLE 4. Basic states related to navigating a tension tower.

Name	Meaning	Figure	State
R_Navigating	The clamping mechanism clamps the ground line and the locking mechanism locks the joint. The robot is not rolling.	Fig. 8(a)	q_0
R_Navi_S1_1	The front clamping mechanism returns home while the rear clamping mechanism clamps the ground line. The front locking mechanism releases and the rear locking mechanism locks the rear locomotion mechanism. The robot is not rolling.	Fig. 8(b)	q_{1_1}
R_Navi_S2_1	The front clamping mechanism returns home while the rear clamping mechanism clamps the ground line. The front locking mechanism releases and the rear locking mechanism locks the rear locomotion mechanism. The robot is rolling forward.	-	q_{2_1}
R_Navi_S3_2	The front clamping mechanism clamps the ground line and the rear clamping mechanism returns home. The rear locking mechanism releases and the front locking mechanism locks the front locomotion mechanism. The robot is not rolling.	Fig. 8(d)	q_{3_2}
R_Navi_S4_2	The front clamping mechanism clamps the ground line and the rear clamping mechanism returns home. The rear locking mechanism releases and the front locking mechanism locks the front locomotion mechanism. The robot is rolling forward.	-	q_{4_2}
R_Travelling	The clamping mechanism clamps the ground line and the locking mechanism locks the joint. The robot is rolling.	Fig. 8(f)	q_5

TABLE 5. Events of the behavior for navigating the first segment of a rail.

Event name	Meaning
σ_1	The approximate switch at the home position of the front clamping mechanism is triggered.
σ_2	Robot command: start the robot.
σ_3	The forward approximate switch of the rear clamping mechanism is triggered.
σ_4	The approximate switch at the home position of the rear clamping mechanism is triggered.
σ_5	Robot command: start the robot.
σ_6	A given time elapses or the approximate switch on the front locomotion mechanism is triggered.
σ_7	The rear clamping mechanism clamps the ground line.

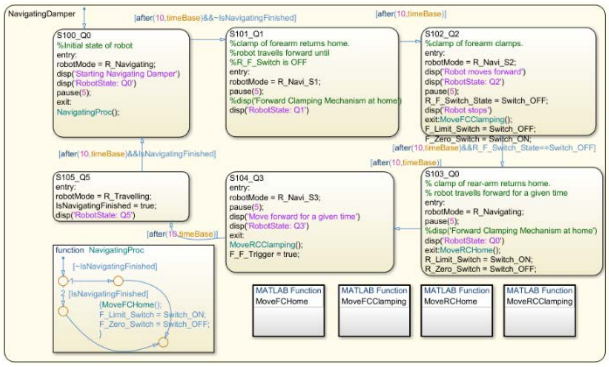

FIGURE 12. Design of the navigating damper state.

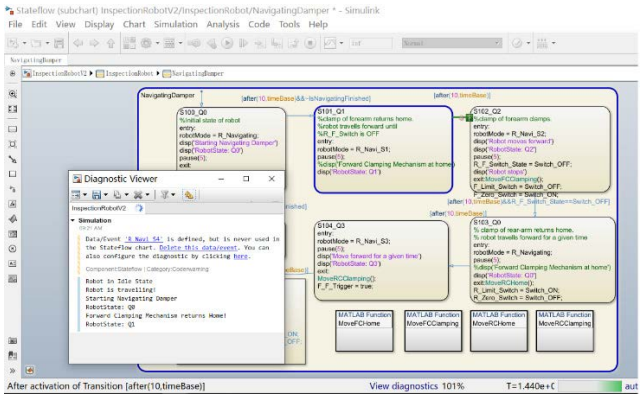

FIGURE 13. Simulation of the model.

such occasions. The robot would stop and control system of the robot would give some prompts. The operator would deal with the error.

The robot may be in exception under other conditions such as the slope of the actual ground line. The slope of the ground line is larger near the tower, where a damper is mounted. Two measures are taken to decrease the possibility of exceptions. Firstly, the mechanical structure is carefully designed and some experiments are conducted to ensure a reliable climbing of the slope. Secondly, there are some extra parameters related to basic behaviors and combinational behaviors, which is helpful for diagnosing the exceptions and errors.

The behaviors are gradually improved by experience and experiments. Human inference is proved to be an effective way to deal with the exceptions.

5) BEHAVIOR PLANNING MODEL AND SIMULATION

The robot system is event driven and the behavior of the system was modeled by describing it in terms of the transitions among robot states using MATLAB/Simulink, as shown in Figure 11. Several constant modules and manual switches

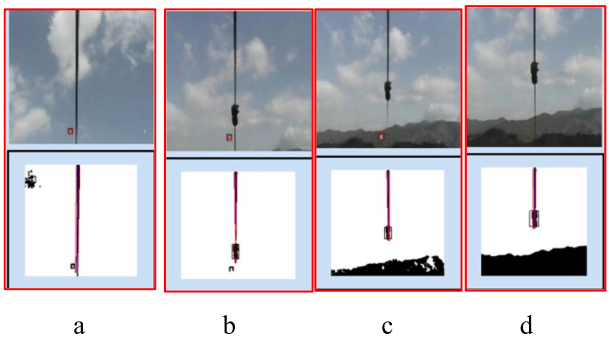

FIGURE 14. Results of the field experiments.

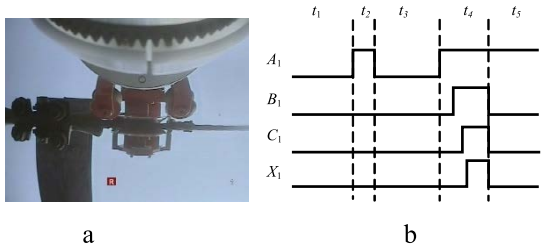

FIGURE 15. Data fusion results.

were used to generate edge-triggered input events to simulate the approximate switches, commands, and outputs of the vision system. Additionally, several logic were used to generate logic input events. Several output signals were simulated to monitor the state of the model.

The key module of the system is the FSM. The robot has four states: idle, normal traveling, navigating damper, and navigating tension tower. The idle state is the default state after the power is turned on and the normal traveling state is a simple state. The robot transitions to a combinational state if a damper or auxiliary rail is detected by the vision system and sensors.

Figure 12 presents the details of the navigating damper state, which is composed of five states and several events. As mentioned previously, the robot takes six steps to navigate a damper. Several MATLAB functions were used to simulate the basic behavior of the robot, such as rolling the front clamping mechanism to its home position.

A simulation was conducted and a diagnostic view was used to monitor the running state of the model, as shown in Figure 13. The outputs of the diagnostic viewer match the normal procedure of the robot for navigating obstacles well, which validates the model.

V. EXPERIMENT

Experiments were conducted in an environment with a mountainous line from a linear tower to a tension tower. The distribution of obstacles along the line was as follows: damper-suspension, clamp-damper-long-distance, ground wire-damper-tension clamp (transition guide rail).

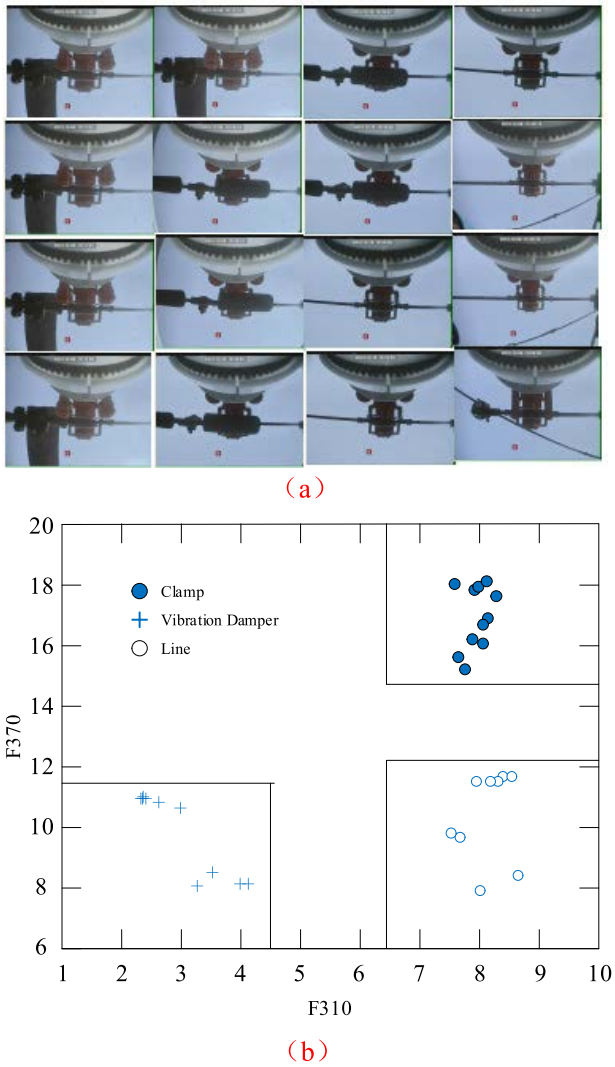

FIGURE 16. Samples and their wavelet moment characteristic distributions.

A. OBSTACLE RECOGNITION TEST

A PTZ camera was installed in front of the robot box and directly below the power line when the robot was rolling. The grayscale information on the line environment in the camera images was used to extract areas suspected of containing obstacles. The images were binarized according to the grayscale features of the wire, suspicious areas were identified through cluster analysis, and suspicious areas were merged, expanded, and shrunk to extract the position of the an obstacle in an image accurately.

Figure 14 presents the results of the field experiments. As shown in Figure 14(a), when the robot PTZ camera detected that the line was unobstructed, the robot rolled forward at high speed (15 m/min). As shown in Figure 14(b), when the robot PTZ camera detected that the distance from the obstacle was 480 cm, the robot began to roll at a speed of $v = v_{\max} \times D/500(D \geq 100\ cm)$. As shown in Figure 14(c), when the PTZ camera detected that the robot was 323 cm

FIGURE 17. Process of vibration damper navigation.

from the obstacle, its rolling speed was reduced to 9.7 m/min. As shown in Figure 14(d), when the PTZ camera detected that the robot was 323 cm from the obstacle, its rolling speed was reduced to 7.6 m/min.

When the robot was <100 cm from the obstacle, it rolled at a low speed and the data from the contact sensor, encoder, and current sensor were fused to detect and locate the obstacle. The robot automatically stopped rolling after contact with the clamp, as shown in Figure 15(a). Figure 15(b) presents the results of data fusion detection with low-speed obstacle location. Area "t_1" indicates that class 3 of the sensors had no action. Area "t_2" indicates the malfunction of the collision sensor. Area "t_4" indicates the occurrence of obstacle collision. Area "t_5" indicates that the robot stopped moving after detecting an obstacle and the contact sensor did not pop up.

In the experiment, 30 images (Figure 16(a)) of each obstacle were captured using a pinhole camera after the obstacles (wires, clamps, and anti-vibration dampers) were located. Figure 16(b) presents the distributions of the wavelet moment features for the three types of obstacles. The distributions of the wavelet moment eigenvalues of the edge images differ significantly between the three obstacles. However, the distribution of eigenvalues for the same type of obstacle is relatively concentrated. Therefore, the three obstacles can be classified and identified.

B. AUTONOMOUS OBSTACLE NAVIGATION EXPERIMENT

Experiments were conducted to verify the effectiveness of the proposed modeling method for navigating obstacles. As shown in Figure 17, the inspection robot navigated the vibration damper automatically. The time required for automatic navigation of the damper was 2 min. The experimental results indicate that the robot can efficiently and automatically navigate typical obstacles in transmission line environments.

VI. CONCLUSION

A novel mobile robot for power transmission line inspection was developed according to the requirements of inspection tasks and characteristics of obstacles on power lines. A prototype was tested and validated under laboratory conditions. According to the requirements for obstacle information accuracy and real-time performance in each stage of autonomous line inspection, a multi-sensor integrated structure for line obstacle location and recognition was proposed. Obstacle location and recognition algorithms for each stage were introduced. According to the characteristics of the obstacles, the current state of the robot was determined by integrating the obstacle detection results and sensor information. Based on the obstacle-crossing process, the state transfer function of each stage was established and behavior planning was completed through state transfers.

REFERENCES

[1] P.-L. Richard, N. Pouliot, F. Morin, M. Lepage, P. Hamelin, M. Lagacc, A. Sartor, G. Lambert, and S. Montambault, "LineRanger: Analysis and field testing of an innovative robot for efficient assessment of bundled high-voltage powerlines," in *Proc. Int. Conf. Robot. Automat. (ICRA)*, May 2019, pp. 9130–9136.

[2] Y. Gao, G. Song, S. Li, F. Zhen, D. Chen, and A. Song, "LineSpyX: A power line inspection robot based on digital radiography," *IEEE Robot. Autom. Lett.*, vol. 5, no. 3, pp. 4759–4765, Jul. 2020.

[3] A. B. Alhassan, X. Zhang, H. Shen, and H. Xu, "Power transmission line inspection robots: A review, trends and challenges for future research," *Int. J. Electr. Power Energy Syst.*, vol. 118, Jun. 2020, Art. no. 105862.

[4] A. T. Zengin, G. Erdemir, T. C. Akinci, and S. Seker, "Measurement of power line sagging using sensor data of a power line inspection robot," *IEEE Access*, vol. 8, pp. 99198–99204, 2020.

[5] A. U. Mahin, S. N. Islam, F. Ahmed, and M. F. Hossain, "Measurement and monitoring of overhead transmission line sag in smart grid: A review," *IET Gener., Transmiss. Distrib.*, vol. 16, no. 1, pp. 1–18, Jan. 2022.

[6] S. Q. Li, "The design and implementation of based on the GPS cable line inspection system," M.S. thesis, Shandong Univ., Jinan, China, 2013.

[7] G. Rui, Z. Feng, C. Lei, and Y. Jun, "A mobile robot for inspection of overhead transmission lines," in *Proc. 3rd Int. Conf. Appl. Robot. Power Ind. (CARPI)*, Oct. 2014, pp. 1–3.

[8] P. Zhu, A. Zhu, Q. Zhang, Y. Wang, X. Zhang, and G. Cao, "Design of gibbon-like crawling robot for high voltage transmission line inspection," in *Proc. 16th Int. Conf. Ubiquitous Robots (UR)*, Jun. 2019, pp. 16–20.

[9] A. T. Zengin, G. Erdemir, T. C. Akinci, F. A. Selcuk, M. N. Erduran, and S. S. Seker, "ROSETLineBot: One-wheel-drive low-cost power line inspection robot design and control," *J. Elect. Syst.*, vol. 15, no. 4, pp. 626–634, 2019.

[10] A. Zhu, Y. Tu, W. Zheng, H. Shen, and X. Zhang, "Design and implementation of high-voltage transmission line inspection and foreign bodies removing robot," in *Proc. 15th Int. Conf. Ubiquitous Robots (UR)*, Jun. 2018, pp. 852–856.

[11] J. Wang, A. Sun, C. Zheng, and J. Wang, "Research on a new crawler type inspection robot for power transmission lines," in *Proc. 1st Int. Conf. Appl. Robot. Power Ind. (CARPI)*, Oct. 2010, pp. 1–5.

[12] L. Huang, G. Wu, J. Liu, S. Yang, Q. Cao, W. Ding, and W. Tang, "Obstacle distance measurement based on binocular vision for high-voltage transmission lines using a cable inspection robot," *Sci. Prog.*, vol. 103, no. 3, pp. 1–35, Jul. 2020.

[13] L. Huang, G. Wu, W. Tang, and Y. Wu, "Obstacle distance measurement under varying illumination conditions based on monocular vision using a cable inspection robot," *IEEE Access*, vol. 9, pp. 55955–55973, 2021.

[14] Z. H. Li, H. G. Wang, Y. C. Wang, Y. Jiang, and X. Yue, "Line-grasping control for a power transmission line inspection robot," *J. Jilin Univ., Eng. Ed.*, vol. 45, no. 5, pp. 1519–1526, 2015.
[15] H. Cao, G. Wu, T. Zheng, and Y. Yan, "Obstacle detection and positioning of autonomous inspection robot for high voltage transmission line," *J. Wuhan Univ., Eng. Ed.*, vol. 45, no. 2, p. 6, 201.
[16] N. Pouliot and S. Montambault, "Field-oriented developments for LineScout technology and its deployment on large water crossing transmission lines," *J. Field Robot.*, vol. 29, no. 1, pp. 25–46, Jan. 2012.
[17] N. Pouliot and S. Montambault, "Geometric design of the LineScout, a teleoperated robot for power line inspection and maintenance," in *Proc. IEEE Int. Conf. Robot. Automat.*, May 2008, pp. 3970–3977.
[18] P. Debenest, M. Guarnieri, K. Takita, E. F. Fukushima, S. Hirose, K. Tamura, A. Kimura, H. Kubokawa, N. Iwama, and F. Shiga, "Expliner–robot for inspection of transmission lines," in *Proc. IEEE Int. Conf. Robot. Automat.*, May 2008, pp. 3978–3984.
[19] G. Wu, T. Zheng, Z. Huang, H. Liu, and C. Li, "Navigation strategy for local autonomous obstacles-overcoming based on magnetic density detection for inspection robot of single split high voltage transmission line," in *Proc. 8th World Congr. Intell. Control Automat. (WCICA)*, Jul. 2010, pp. 6555–6561.
[20] H. Wang, F. Zhang, Y. Jiang, G. Liu, and X. Peng, "Development of an inspection robot for 500 kV EHV power transmission lines," in *Proc. IEEE/RSJ Int. Conf. Intell. Robots Syst. (IROS)*, Oct. 2010, pp. 5107–5112.
[21] W. B. Guo, H. G. Wang, Y. Jiang, and A. H. Liu, "Obstacle navigation planning for a power transmission line inspection robot," *Robot*, vol. 34, no. 4, pp. 505–512, 2012.
[22] F. Charbonnier, H. Alla, and R. David, "Discrete-event dynamic systems," *IEEE Trans. Control Syst. Technol.*, vol. 7, no. 2, pp. 175–187, Mar. 1999.
[23] P. J. Ramadge and W. M. Wonham, "Supervisory control of a class of discrete event processes," *SIAM J. Control Optim.*, vol. 25, no. 1, pp. 206–230, Jan. 1987.
[24] X. H. Xu, L. G. Dai, and Y. P. Li, "The latest development of DEDS monitoring theory," *Control Decis.*, vol. 12, no. A00, p. 7, 1997.
[25] Y. F. Song, H. G. Wang, Z. H. Li, and Y. Jiang, "Vision based transmission line broken strand detection and robot behaviour planning," *Robot*, vol. 37, no. 2, pp. 204–211 and 223, 2015.
[26] M. Steenstrup, M. A. Arbib, and E. G. Manes, "Port automata and the algebra of concurrent processes," *J. Comput. Syst. Sci.*, vol. 27, no. 1, pp. 29–50, Aug. 1983.

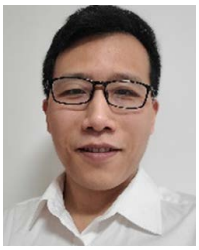

XIANG YUE was born in Jining, Shandong, China, in 1986. He received the B.S. degree in mechanical design, manufacturing, and automation from the Shenyang University of Technology, Shenyang, Liaoning, China, in 2010, and the Ph.D. degree in pattern recognition and intelligent systems from the Shenyang Institute of Automation (SIA), Chinese Academy of Sciences, Shenyang, in 2017.

Since 2017, he has been a Lecturer at Shenyang Agricultural University, Shenyang. His research interests include electric powered robots and intelligent agricultural equipment.

YAN FENG was born in Tongliao, Inner Mongolia, China, in 1998. He received the Bachelor of Engineering degree in agricultural engineering from Shenyang Agricultural University, in 2021, where he is currently pursuing the master's degree in agricultural engineering and information technology.

BINZHANG JIANG, photograph and biography not available at the time of publication.

LIN WANG was born in Yichang, Hubei, China, in 1987. He received the B.S. degree in mechanical engineering from the Huazhong University of Science and Technology, Wuhan, in 2010, and the Ph.D. degree in mechanical engineering from the Shenyang Institute of Automation (SIA), Chinese Academy of Sciences, Shenyang, in 2017.

Since 2017, he has been a Lecturer at the Changshu Institute of Technology, Changshu, Jiangsu, China. His research interests include power transmission line inspection, maintenance robots, and intelligent manufacturing.

JUNMING HOU was born in Shenyang, China. He received the M.S. and Ph.D. degrees in mechanical manufacturing and automation from the School of Mechanical Engineering and Automation, Northeastern University, China, in 2006 and 2009, respectively. He is currently an Associate Professor with the School of Engineering, Shenyang Agricultural University, China. His research interests include general machinery design, agricultural machinery design, biological system engineering, agricultural product harvesting and processing technology, and fruit production machinery.